A MeerKAT survey of nearby nova-like cataclysmic variables

D. M. Hewitt [1,2]★ M. L. Pretorius,[1] P. A. Woudt,[2] E. Tremou,[3]
J. C. A. Miller-Jones [4] C. Knigge,[5] N. Castro Segura [5] D. R. A. Williams [6,7]
R. P. Fender,[2,6] R. Armstrong,[8,9] P. Groot,[1,2,10] I. Heywood [6,9,11] A. Horesh,[12]
A. J. van der Horst,[13,14] E. Koerding,[10] V. A. McBride,[1,2,15] K. P. Mooley [16,17,18]
A. Rowlinson [19,20] B. Stappers[7] and R. A. M. J. Wijers [19]

[1] *South African Astronomical Observatory, PO Box 9, Observatory 7935, Cape Town, South Africa*
[2] *Department of Astronomy, University of Cape Town, Private Bag X3, Rondebosch 7701, South Africa*
[3] *LESIA, 5 place Jules Janssen, Observatoire de Paris, CNRS, PSL, Meudon 92195, France*
[4] *International Centre for Radio Astronomy Research - Curtin University, GPO Box U1987, Perth, WA 6845, Australia*
[5] *School of Physics and Astronomy, University of Southampton, Highfield, Southampton SO17 1BJ, UK*
[6] *Department of Physics, Astrophysics, University of Oxford, Denys Wilkinson Building, Keble Road, Oxford OX1 3RH, UK*
[7] *Department of Physics and Astronomy, Jodrell Bank Centre for Astrophysics, The University of Manchester, Manchester M13 9PL, UK*
[8] *Department of Astronomy, Inter-University Institute for Data Intensive Astronomy, University of Cape Town, Private Bag X3, Rondebosch 7701, South Africa*
[9] *South African Radio Astronomy Observatory, 2 Fir Street, Black River Park, Observatory, Cape Town 7925, South Africa*
[10] *Department of Astrophysics/IMAPP, Radboud University Nijmegen, PO Box 9010, NL-6500 GL Nijmegen, the Netherlands*
[11] *Department of Physics and Electronics, Rhodes University, PO Box 94, Makhanda 6140, South Africa*
[12] *Racah Institute of Physics, The Hebrew University of Jerusalem, Jerusalem 91904, Israel*
[13] *Department of Physics, The George Washington University, 725 21st Street NW, Washington, DC 20052, USA*
[14] *Astronomy, Physics and Statistics Institute of Sciences (APSIS), 725 21st Street NW, Washington, DC 20052, USA*
[15] *Office of Astronomy for Development, IAU, Cape Town 7935, South Africa*
[16] *Department of Physics, University of Oxford, Keble Road, Oxford OX1 3RH, UK*
[17] *National Radio Astronomy Observatory, Socorro, NM 87801, USA*
[18] *Caltech, 1200 E. California Blvd. MC 249-17, Pasadena, CA 91125, USA*
[19] *Anton Pannekoek Institute, University of Amsterdam, Postbus 94249, NL-1090 GE Amsterdam, the Netherlands*
[20] *Netherlands Institute for Radio Astronomy (ASTRON), Oude Hoogeveensedijk 4, NL-7991 PD Dwingeloo, the Netherlands*

ABSTRACT

We present the results of MeerKAT radio observations of 11 nearby nova-like cataclysmic variables (CVs). We have detected radio emission from IM Eri, RW Sex, V3885 Sgr, and V603 Aql. While RW Sex, V3885 Sgr, and V603 Aql had been previously detected, this is the first reported radio detection of IM Eri. Our observations have doubled the sample of non-magnetic CVs with sensitive radio data. We observe that at our radio detection limits, a specific optical luminosity $\gtrsim 2.2 \times 10^{18}$ erg s^{-1} Hz^{-1} (corresponding to $M_V \lesssim 6.0$) is required to produce a radio detection. We also observe that the X-ray and radio luminosities of our detected nova-like CVs are on an extension of the $L_X \propto L_R^{\sim 0.7}$ power law originally proposed for non-pulsating neutron star low-mass X-ray binaries. We find no other correlations between the radio emission and emission in other wavebands or any other system parameters for the existing sample of radio-detected non-magnetic CVs. We measure in-band (0.9–1.7 GHz) radio spectral indices that are consistent with reports from earlier work. Finally, we constructed broad spectral energy distributions for our sample from published multiwavelength data, and use them to place constraints on the mass transfer rates of these systems.

Key words: accretion, accretion discs – stars: jets – novae, cataclysmic variables – white dwarfs – radio continuum: stars – X-rays: binaries.

★ E-mail: dantehewitt@gmail.com, dante@saao.ac.za, retha@saao.ac.za

1 INTRODUCTION

Cataclysmic variables (CVs) are semidetached binary star systems in which a white dwarf (WD) accretes mass from a late-type main-sequence star (usually a K- or M-type red dwarf star) via Roche lobe overflow (Warner 1995). The accretion flow geometry is largely governed by the magnetic field strength (B) of the WD. In the case where $B \lesssim 10^5$ G (e.g. Coppejans & Knigge 2020), these systems are termed 'non-magnetic' CVs and accretion occurs via an accretion disc. In non-magnetic CVs, the mass transfer rate ($\dot{M}$) regulates the stability of the accretion disc. For $\dot{M} \lesssim 10^{-9}$ M$_\odot$ yr^{-1}, the accretion disc is unstable and thermal-viscous instabilities can switch the disc between faint and bright states (the disc instability model; e.g. Osaki 1974). This is also the same mechanism believed to be responsible for triggering the outbursts of low-mass X-ray binaries (XRBs; e.g. Coriat, Fender & Dubus 2012). These episodic outbursts are called dwarf nova outbursts and CVs that display them are known as dwarf novae (DNe). In CVs, a mass transfer rate of $\dot{M} \gtrsim 10^{-9}$ M$_\odot$ yr^{-1} is sufficient to sustain the accretion disc in a perpetual hot state (Osaki 1996, but note that the critical $\dot{M}$ distinguishing between stable discs and those subject to the disc instability depends on the size of the disc, and hence on orbital period). Those high-$\dot{M}$ systems will have stable accretion discs and will not show DN outbursts. Non-magnetic CVs in which DN outbursts are not observed are termed nova-like CVs (NLs).

Accreting compact objects, ranging over numerous orders of magnitude in mass, are known to launch jets. WDs represent the weak-field gravity regime and are thus an important test case for this so-called *disc–jet coupling*. Jet launching has been observed in various classes of accreting WDs, including symbiotic stars (e.g. Taylor, Seaquist & Mattei 1986), supersoft sources (e.g. Tomov et al. 1998), and post-nova eruption systems (e.g. Sokoloski, Rupen & Mioduszewski 2008). More recently, it has been shown that non-magnetic CVs are also an important class of radio emitters (Coppejans et al. 2015, 2016). While in many cases the observed radio emission from non-magnetic CVs can be described by synchrotron emission relating to a jet, some ambiguity remains (see Coppejans & Knigge 2020 for a review on CVs and jets).

Initial surveys to detect radio emission from the non-magnetic CVs, including the NLs RW Sex and TT Ari (Cordova, Hjellming & Mason 1983; Nelson & Spencer 1988), V603 Aql (Fuerst et al. 1986), and MV Lyr (Nelson & Spencer 1988) were unsuccessful. Radio emission was, however, detected in a few DNe such as SU UMa (Benz, Fürst & Kiplinger 1983) and SS Cyg (Körding et al. 2008; Miller-Jones et al. 2011; Russell et al. 2016; Mooley et al. 2017; Fender et al. 2019), but only in the latter were reproducible outbursts seen.

The first reproducible radio detection of a NL was presented by Körding et al. (2011), who detected the NL V3885 Sgr with the Australia Telescope Compact Array (ATCA) at 5.5 GHz. They also observed, but did not detect AC Cnc and IX Vel. Prior to these observations, the only other reported detection of a NL in the radio regime had been that of AC Cnc (Torbett & Campbell 1987). Re-reduction and re-analysis of these data, however, showed a positional offset of 14 arcsec, making the original detection implausible (Körding et al. 2011).

Coppejans et al. (2015) observed four NLs with the Karl G. Jansky Very Large Array (VLA) at 6 GHz and detected three NLs in two epochs: RW Sex, V603 Aql, and TT Ari, thus doubling the number of non-magnetic CVs detected at radio wavelengths. V1084 Her was not detected in either epoch and the authors noted that due to the poor constraints on the distance (305 ± 137 pc at the time;

Ak et al. 2008) it is not clear if the system is too far away or simply intrinsically radio faint. From *Gaia* DR2, we now know the distance to V1034 Her is 444.3 ± 5.8 pc, making the former explanation more likely. Coppejans et al. (2015, 2016) came to the conclusion that the reason for the plethora of previous non-detections was a lack of sensitivity.

Various radio emission mechanisms have been proposed for the NLs. Optically thick synchrotron emission, gyrosynchrotron emission, or cyclotron maser emission have been suggested as possible radio emission mechanisms by Coppejans et al. (2015), while Körding et al. (2011) argued that the emission observed from V3885 Sgr is best described as optically thin synchrotron emission.

In addition to our poor knowledge regarding the radio emission mechanism(s) in NLs, many uncertainties in the physics behind radio emission from these systems remain. To date, no correlation between the radio emission and any system parameters or emission in other wavebands has been found. Motivated by the need for a larger sample of radio-detected NLs to identify any possible correlations, and to shed more light on the radio properties of accreting WDs, we have conducted a survey of NLs using the MeerKAT radio interferometer (Meer Karoo Array Telescope; Jonas 2009).

In Section 2, we describe the selection criteria for the sample of NLs, and briefly overview each system. Details regarding the radio observations and data reductions are discussed in Section 3. In Section 4, the results of these radio observations are presented and discussed. Section 5 summarizes our main findings.

2 THE VOLUME-LIMITED NL SAMPLE

Our sample consists of known southern NLs with measured orbital periods within 350 pc. We selected a sample of NLs from a catalogue of known CVs and CV candidates made available to us by E. Breedt through private communication. This catalogue was compiled from various sources including transient surveys and ATels,[1] consisting of ~8000 objects as of 2018 April 24. Four selection criteria were implemented for the sample: systems classified as NLs, systems with known orbital periods, systems with *Gaia* DR2 distances <350 pc and systems with declinations <+10°. This resulted in a sample of 11 NLs.

This sample includes a few systems that have not been very well studied. It is possible that, with long-term photometric monitoring, one or two may turn out to be DNe.

In Table 1, the optical coordinates, distance estimates, orbital periods, and detected magnitude range of the target systems are given. We will now briefly discuss each of these systems in order of increasing distance, focusing on their most prominent features and any previous radio observations.

2.1 IX Vel

IX Vel is the brightest CV in the night sky, with $V \sim 9.5$. Extensive studies of this system have yielded numerous system parameters, including the masses of the WD (M_1) and secondary companion (M_2): $M_1 = 0.80^{+0.16}_{-0.11}$ M$_\odot$ and $M_2 = 0.52^{+0.10}_{-0.07}$ M$_\odot$ (Beuermann & Thomas 1990), a mass transfer rate of $\dot{M} = 5 \times 10^{-9}$ M$_\odot$ yr^{-1} and an inclination of $i = 57° \pm 2°$ (Linnell et al. 2007). Ultraviolet spectra of IX Vel reveal a P Cygni profile associated with wind outflows of ~3000 km s^{-1} (e.g. Sion 1985).

[1] Astronomer's Telegram: http://www.astronomerstelegram.org.

Table 1. Optical coordinates, distances, orbital periods, and observed *V*-band magnitude ranges for the NLs in our sample. The coordinates and distance measurements are from *Gaia* DR2 (Gaia Collaboration 2016, 2018; Luri et al. 2018), and the magnitude ranges from The International Variable Star Index (VSX).

Target name	RA (J2000)	Dec. (J2000)	Distance (pc)	Orbital period (d)	*V*-band magnitude Range[2]	Absolute magnitude Range	Orbital period reference
IX Vel	$08^h15^m19^s.0$	$-49°13'20''.7$	90.6 ± 0.2	0.193929(2)	9.1–10.0	4.3–5.2	Beuermann & Thomas (1990)
V3885 Sgr	$19^h47^m40^s.5$	$-42°00'26''.4$	132.7 ± 1.4	0.20716071(22)	10.3–10.5	4.7–4.9	Ribeiro & Diaz (2007)
V341 Ara	$16^h57^m41^s.5$	$-63°12'38''.4$	156.1 ± 2.0	0.15216(2)	10.4–12.5	4.4–6.5	Bond & Miszalski (2018)
V5662 Sgr	$20^h05^m51^s.2$	$-29°34'58''.0$	168.6 ± 5.2	0.062887(37)	15.4–18.0	9.3–11.9	Tappert, Augusteijn & Maza (2004)
IM Eri	$04^h24^m41^s.1$	$-20°07'11''.8$	191.2 ± 1.4	0.1456348(4)	11.1–13.3	4.7–6.9	Armstrong et al. (2013)
LS IV -08 3	$16^h56^m29^s.6$	$-08°34'38''.7$	211.0 ± 2.8	0.1952894(10)	11.3–11.6	4.7–5.0	Stark et al. (2008)
RW Sex	$10^h19^m56^s.4$	$-08°41'56''.1$	236.5 ± 5.0	0.24507(20)	10.4–10.8	3.5–3.9	Beuermann, Stasiewski & Schwope (1992)
UU Aqr	$22^h09^m05^s.8$	$-03°46'17''.7$	255.9 ± 5.1	0.1638049430	12.9–15.5	5.9–8.5	Baptista & Bortoletto (2008)
V347 Pup	$06^h10^m33^s.7$	$-48°44'25''.4$	295.8 ± 1.4	0.231936060(6)	13.4–15.8	6.0–8.4	Thoroughgood et al. (2005)
V603 Aql	$18^h48^m54^s.6$	$00°35'02''.9$	313.4 ± 6.7	0.1382009(4)	-0.5^a–12.7	-8.0^a–5.2	Peters & Thorstensen (2006)
CM Phe	$00^h21^m33^s.2$	$-51°42'34''.6$	315.1 ± 3.8	0.2689(7)	14.8–15.8	7.3–8.3	Hoard, Wachter & Kim-Quijano (2001)

^{a}The nova eruption of 1918.

IX Vel was observed in 2008 in the radio band using the ATCA in the 6A configuration, with a maximum baseline of 6-km. Due to a bright nearby source, noise levels were too high to yield anything other than an upper limit of 0.6 mJy (Körding et al. 2011).

2.2 V3885 Sgr

V3885 Sgr is the first NL in which spiral structure in the accretion disc was detected via Doppler tomography (Hartley et al. 2005). In the same work, they constrained the mass ratio of V3885 Sgr to $q = M_2/M_1 \gtrsim 0.7$, proposing mass limits for the primary $0.55\,M_\odot < M_1 < 0.80\,M_\odot$ and an inclination $i > 65°$. These mass constraints were confirmed by Ribeiro & Diaz (2007), who also estimated the inclination to be within the interval $45° < i < 75°$. A mass transfer rate of $\dot{M} = (5.0 \pm 2.0) \times 10^{-9}\,M_\odot\,yr^{-1}$ in combination with parameter values that fall within the above-mentioned ranges can reproduce the combined *Far Ultraviolet Spectroscopic Explorer* and Space Telescope Imaging Spectrograph spectra of V3885 Sgr (Linnell et al. 2009).

V3885 Sgr has been observed using ATCA in 2008 and again in 2010 (Körding et al. 2011). In 2008, it was detected at 4.4σ with a flux density of 0.12 ± 0.03 mJy at 4.8 and 4.9 GHz. The 2010 observations detected the source at 5.5 GHz (17σ) and 9 GHz (7σ) with flux densities of 0.16 ± 0.01 mJy and 0.11 ± 0.02 mJy, respectively. The emission had a spectral index $\alpha \sim -0.75$ (where $S_\nu \propto \nu^\alpha$) and was not variable.

2.3 V341 Ara

The relatively poorly studied V341 Ara is a NL system that is surrounded by both a faint $H\alpha$ nebula, designated Fr 2-11 (Frew 2008), as well as a bow shock nebula (Bond & Miszalski 2018). Bond & Miszalski (2018) attribute the origin of this bow shock nebula to either the system undergoing a high-speed chance encounter with an interstellar gas cloud or the nebula in fact being the remaining ejecta from a previous nova outburst. A recent multiwavelength campaign (Castro Segura, in preparation) has established many fundamental properties of the system. There are no previous accounts of radio observations of V341 Ara in the literature.

2.4 V5662 Sgr

V5662 Sgr is a faint and little-studied system, with the shortest orbital period in our sample. Tappert et al. (2004) noted an unusually strong $H\alpha$ emission line, and suggested that this system may be a DN in which outbursts have been missed. The literature contains no reported observations of V5662 Sgr in the radio regime.

2.5 IM Eri

IM Eri is a non-eclipsing NL system that shows blue-shifted He I 5876, commonly associated with strong wind outflows (Armstrong et al. 2013). Additionally both superorbital and suborbital frequencies have been measured (Armstrong et al. 2013), suggesting an accretion disc tilted with respect to the orbital plane. No observations of IM Eri at radio wavelengths have been reported.

2.6 LS IV -08 3

LS IV -08 3 is an optically bright system classified as an NL (Stark et al. 2008) with no previously reported radio observations.

2.7 RW Sex

RW Sex is well studied and optically bright non-eclipsing NL with a derived mass ratio of $q = 0.74 \pm 0.10$ and system inclination between $28° < i < 40°$ (Beuermann et al. 1992). Linnell et al. (2010) estimated a mass transfer rate of $\dot{M} \sim 5 \times 10^{-9}\,M_\odot\,yr^{-1}$. The spectrum of the secondary star is best fitted by that of a K5 dwarf (Vande Putte et al. 2003). No optical features associated with collimated outflows have been found[2] down to an equivalent width of ~ 0.015 Å (Hillwig, Livio & Honeycutt 2004), but there is evidence for a significant disc wind (~ 4550 km s^{-1}) in the system (e.g Prinja & Rosen 1995).

RW Sex has previously been observed at radio wavelengths by Cordova et al. (1983) and Coppejans et al. (2015). Cordova et al. observed, but did not detect, RW Sex with the pre-upgrade

[2]https://www.aavso.org/vsx/index.php

Table 2. Radio observations log.

Name	Start date and time (UTC)	Primary calibrator	Secondary calibrator	Integrated time on target (s)	Number of antennas
IX Vel	2018 Oct 31 00:44:37.1	J0408-6545	J0825-5010	6246	61
V3885 Sgr	2018 Oct 30 18:28:54.6	J1939-6342	J1937-3958	6253	61
V341 Ara	2019 Mar 29 00:13:21.9	J1939-6342	J1726-5529	7183	60
V5662 Sgr	2019 Apr 01 03:18:49.0	J1939-6342	J1924-2914	8069	60
IM Eri	2019 Mar 30 10:20:54.6	J0408-6545	J0409-1757	8084	60
LS IV -08 3	2019 Mar 29 00:30:25.5	J1939-6342	J1733-1304	6294	60
RW Sex	2019 Mar 31 22:46:05.9	J1331+3030	J1058+0133	6293	60
UU Aqr	2019 June 28 23:06:45.8	J1939-6342	J2225-0457	7180	62
V347 Pup	2019 June 27 09:06:10.7	J0408-6545	J0538-4405	6285	60
V603 Aql	2019 Feb 26 03:10:14.2	J1939-6342	J1911-2006	5367	61
CM Phe	2019 June 29 01:29:22.1	J1939-6342	J2357-5311	7198	62
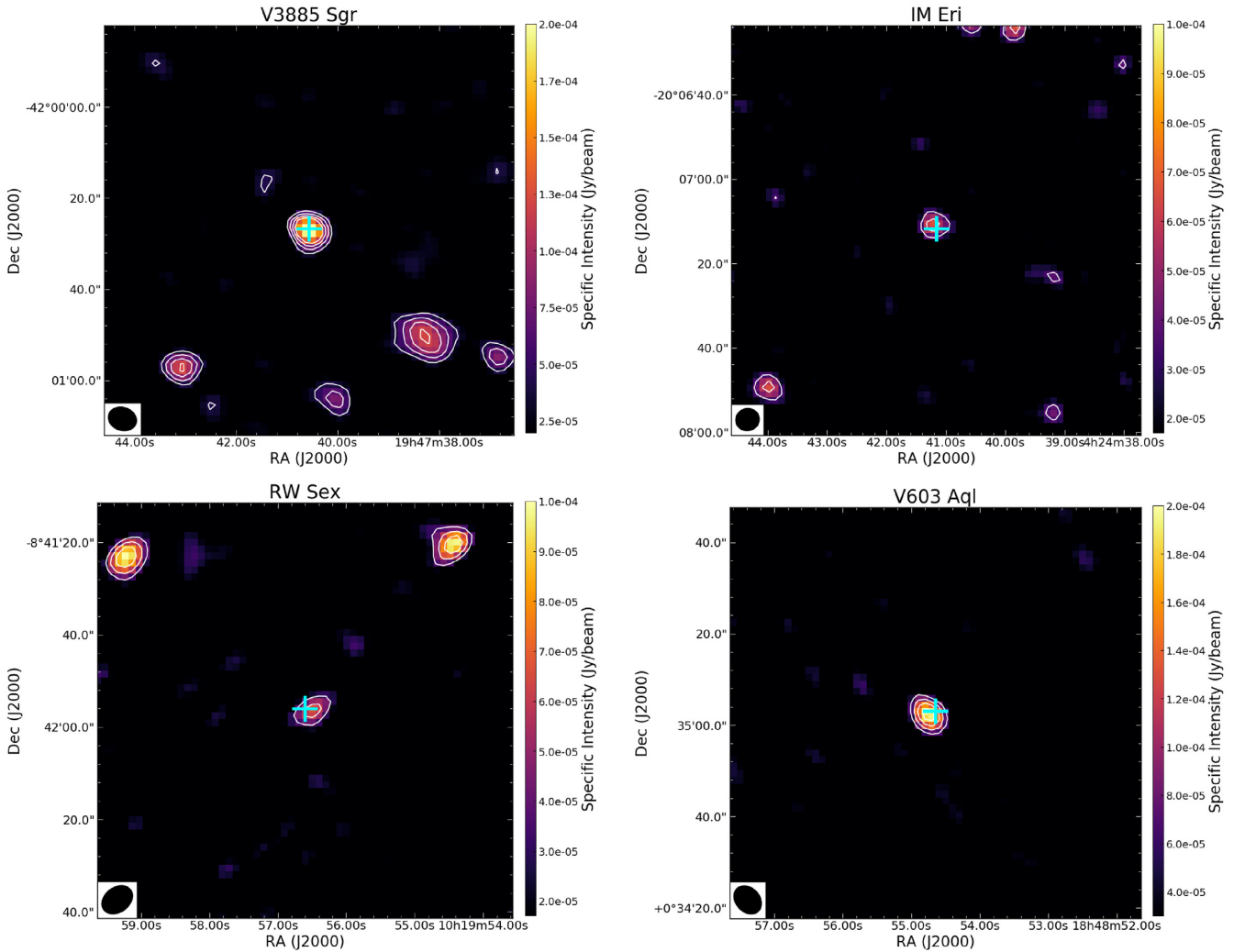
Figure 1. Radio colour maps and contours of the four NLs that we detected with MeerKAT. Contour levels are at 3σ, 5σ, 7σ, and 9σ levels. The cyan plus indicates the position of the optical coordinates and does not correspond to the error bars. These images are 1.5 arcmin × 1.5 arcmin in size and the shape of the beam is shown in the bottom left corner. Refer to Table 3 for beam dimensions. North is up and east to the left.

VLA at 4.885 GHz with a 50 MHz bandwidth. An upper limit of 0.15 mJy is given. Coppejans et al. (2015) observed RW Sex in two epochs with the VLA in the A configuration at 6 GHz with a 4 GHz bandwidth. They detected RW Sex in both epochs with peak flux densities of 33.6 μJy (rms noise 3.7 μJy beam^{-1}) and 26.8 μJy (rms noise 3.3 μJy beam^{-1}), respectively. A spectral index of $\alpha = -0.5 \pm 0.7$ was calculated and no variability was observed over the ~20 min observation. They propose gyrosynchrotron emission,

Table 3. Results from radio observations.

Name	Beam size (arcsec)	Beam position angle (°)	Integrated radio flux Density (μJy)	Radio luminosity ($\times 10^{15} \mathrm{erg\,s^{-1}\,Hz^{-1}}$)	RMS (μJy beam^{-1})	Spectral index
IX Vel	5.9 × 4.1	−50.3	<42	<0.4	14	
V3885 Sgr	6.6 × 5.2	38.6	256 ± 25	5.4 ± 0.5	13	−0.6 ± 0.7
V341 Ara	5.9 × 4.6	−15.1	<27	<0.8	9	
V5662 Sgr	5.3 × 4.5	−25.7	<24	<0.8	8	
IM Eri	5.7 × 5.3	−73.9	99 ± 26	4.3 ± 1.1	11	1.2 ± 1.6
LS IV -08 3	5.8 × 4.7	−8.1	<33	<1.8	11	
RW Sex	6.4 × 5.0	−55.0	82 ± 23	5.5 ± 1.6	11	−1.5 ± 1.0
UU Aqr	6.1 × 5.5	9.0	<39	<3.1	13	
V347 Pup	5.7 × 4.5	−6.8	<30	<3.1	10	
V603 Aql	6.9 × 5.3	42.4	233 ± 36	27 ± 4	20	0.2 ± 1.1
CM Phe	6.2 × 4.5	−39.2	<30	<4.6	10	
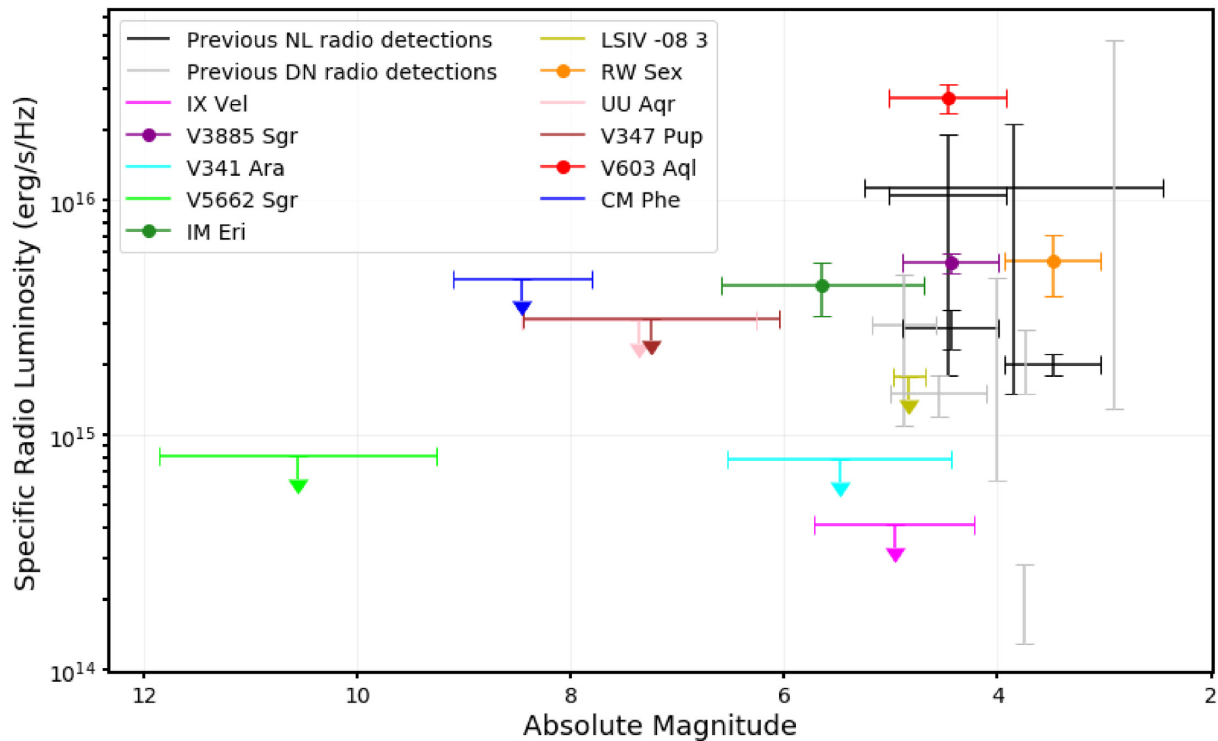
Figure 2. Specific radio luminosities plotted versus the absolute magnitudes for this sample of 11 NLs, with the *y*-error bars corresponding to the radio luminosity uncertainty and *x*-error bars to the magnitude range obtained from the Ritter–Kolb catalogue (Ritter & Kolb 2003), or VSX if not available from the former. All previous radio defections of DNe and NLs have also been plotted in grey and black, respectively (Körding et al. 2008; Miller-Jones et al. 2011; Coppejans et al. 2015, 2016; Russell et al. 2016; Barrett et al. 2017; Pala 2019; Coppejans & Knigge 2020). For these data points, the *y*-error bars represent the minimum and maximum luminosities at which these sources have been detected in the radio regime, while the *x*-error bars represent the normal magnitude range for NLs and maximum magnitude during outburst/superoutburst for DNe. Note that the radio luminosities of our sample are not at the same frequency as that of previous detections.

cyclotron maser emission, and optically thin synchrotron emission as possible emission mechanisms, favouring the latter.

2.8 UU Aqr

UU Aqr is an eclipsing NL with a mass ratio $q = 0.30 \pm 0.07$, $M_1 = 0.67 \pm 0.14\,\mathrm{M_\odot}$, $M_2 = 0.20 \pm 0.07\,\mathrm{M_\odot}$, an inclination $i = 78° \pm 2°$, and a K7-M0 spectral type for the secondary star (Baptista, Steiner & Cieslinski 1994). Baptista, Steiner & Horne (1996) estimate $\dot{M} = 10^{-9.0\pm0.2}\,\mathrm{M_\odot\,yr^{-1}}$.

UU Aqr displays various forms of variability, ranging from 'stunted' DN oubursts that cause short-term variability (of up to a magnitude) on a time-scale of days (Honeycutt, Robertson & Turner 1998) to long-term variability (≈0.3 mag) on a time-scale of years (Baptista et al. 1994). Additionally, Baptista et al. (1994) reported bright flares that can constitute up to a quarter of the total system brightness. The principal source of flickering in UU Aqr is explained as spiral shocks in the outer accretion disc induced by tidal interactions from the secondary star (Baptista & Bortoletto 2008). No radio observations of UU Aqr have been reported.
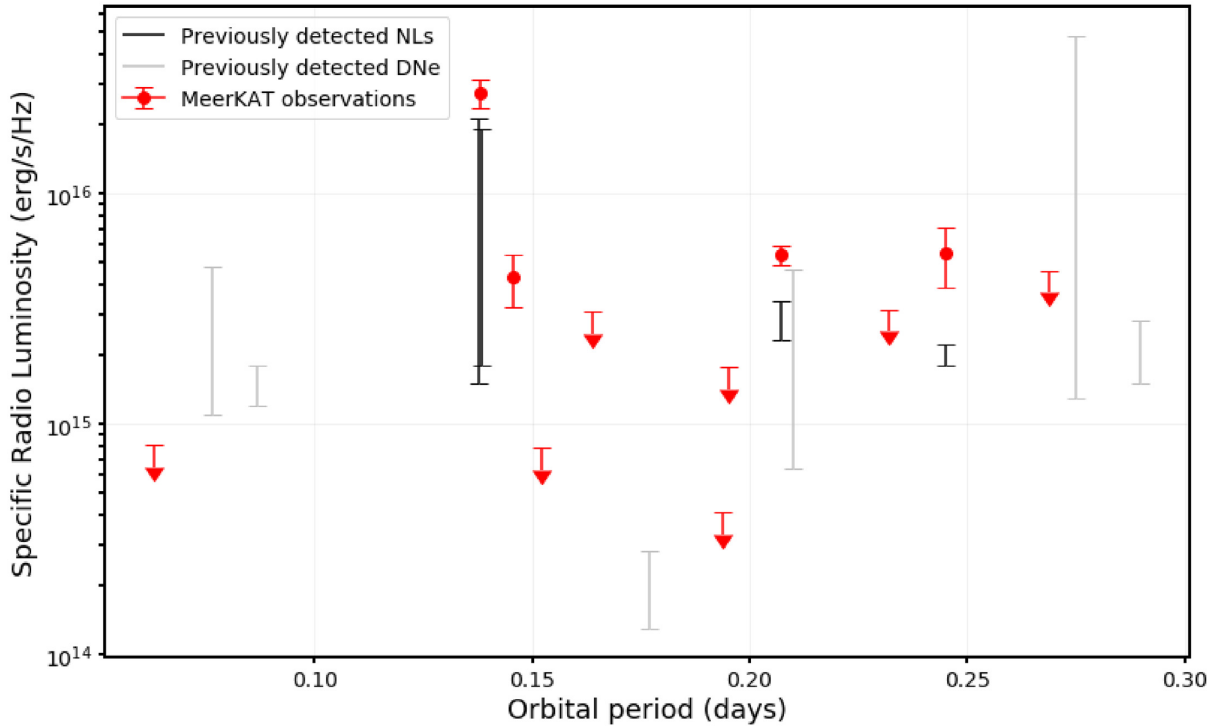
Figure 3. Specific radio luminosities of non-magnetic CVs as a function of orbital periods. The red symbols are for this sample of 11 NLs, with the *y*-error bars corresponding to the radio luminosity uncertainty. Previously reported data are shown for DNe (the grey symbols) and NLs (black), where again the bars represent a range of measured radio luminosities (Körding et al. 2008; Miller-Jones et al. 2011; Coppejans et al. 2015, 2016; Russell et al. 2016; Barrett et al. 2017; Pala 2019; Coppejans & Knigge 2020). As with Fig. 2, note that the radio luminosities of our sample are not at the same frequency as that of previous detections.

2.9 V347 Pup

V347 Puppis was classified as an eclipsing NL system by Buckley et al. (1990). The authors noted this system could be an intermediate polar, partly due to the large L_x/L_{opt} ratio, and that this will have to be resolved by searching for coherent optical pulsations. To our knowledge, no coherent optical pulsations have been found to date, and there is no strong evidence in the literature that this system is magnetic. Spiral structure in the accretion disc was first reported by Still, Buckley & Garlick (1998). Multiple system parameters for V347 Pup were derived by Thoroughgood et al. (2005): a mass ratio $q = 0.83 \pm 0.05$, $M_1 = 0.63 \pm 0.04\,M_\odot$, $M_2 = 0.52 \pm 0.06\,M_\odot$, inclination $i = 84°0 \pm 2°3$, and a M0.5V spectral type for the secondary star, and the authors also confirmed the presence of the aforementioned spiral structure. There are no reported observations of V347 Pup in the radio regime to date.

2.10 V603 Aql

In 1918, V603 Aql (or Nova Aquilae 1918) rose to a magnitude of -0.5 during a nova eruption, making it the brightest nova eruption of the 20th century (e.g. Payne-Gaposchkin 1964; Johnson et al. 2014). A mass ratio of $q = 0.24 \pm 0.05$, stellar masses of $M_1 = 1.2 \pm 0.2\,M_\odot$ and $M_2 = 0.29 \pm 0.04\,M_\odot$, and an inclination of $i = 13° \pm 2°$ have been estimated by Arenas et al. (2000). Retter & Naylor (2000) estimated $\dot{M}$ between $9.2 \times 10^{-9}\,M_\odot\,yr^{-1}$ and $9.47 \times 10^{-8}\,M_\odot\,yr^{-1}$.

V603 Aql has previously been observed in the radio regime by Coppejans et al. (2015), as well as Barrett et al. (2017). The first

authors took two observations in the 4–8 GHz band with the VLA in the A configuration during April 2014. In the first epoch, the emission displayed a spectral index of $\alpha = 0.54 \pm 0.05$ and a peak flux density of 178.2 μJy (rms noise 4.3 μJy beam^{-1}) and in the second, a week later, $\alpha = 0.16 \pm 0.08$ with a peak flux density of 190.5 μJy (rms noise 3.9 μJy beam^{-1}). During the first observation, short term variability down to a time scale of 217 s was found, but V603 Aql was not variable in the second observation. The peak amplitude of the variability was 61 μJy. The authors note that the radio emission observed is consistent with gyrosynchrotron emission, cyclotron maser emission, and optically thick synchrotron emission.

V603 Aql was also observed twice in 2013 with the VLA in the 4–6, 8–10, and 18–22 GHz bands (Barrett et al. 2017). The authors note that the measured flux densities may be in error because 3C 295 (a radio source that is spatially resolved at high frequencies, and with no calibration models) was used as a flux standard. It was detected once in the 4–6 GHz band (24 ± 8 μJy), twice in the 8–10 GHz band (51 ± 20 μJy and 79 ± 14 μJy), and not at all in the 18–22 GHz band. Following the discussion in Barrett et al. (2017), should the source not be detected, 3σ-upper limits for the 4–6, 8–10, and 18–22 GHz bands are 75, 75, and 99 μJy, respectively.

2.11 CM Phe

CM Phe is a faint system that has historically been notoriously difficult to locate. Jaidee & Lyngå (1969) correctly identified it while observing a fainter star located a few arcminutes away from L218-28 (the object mistaken for CM Phe for many years). Based
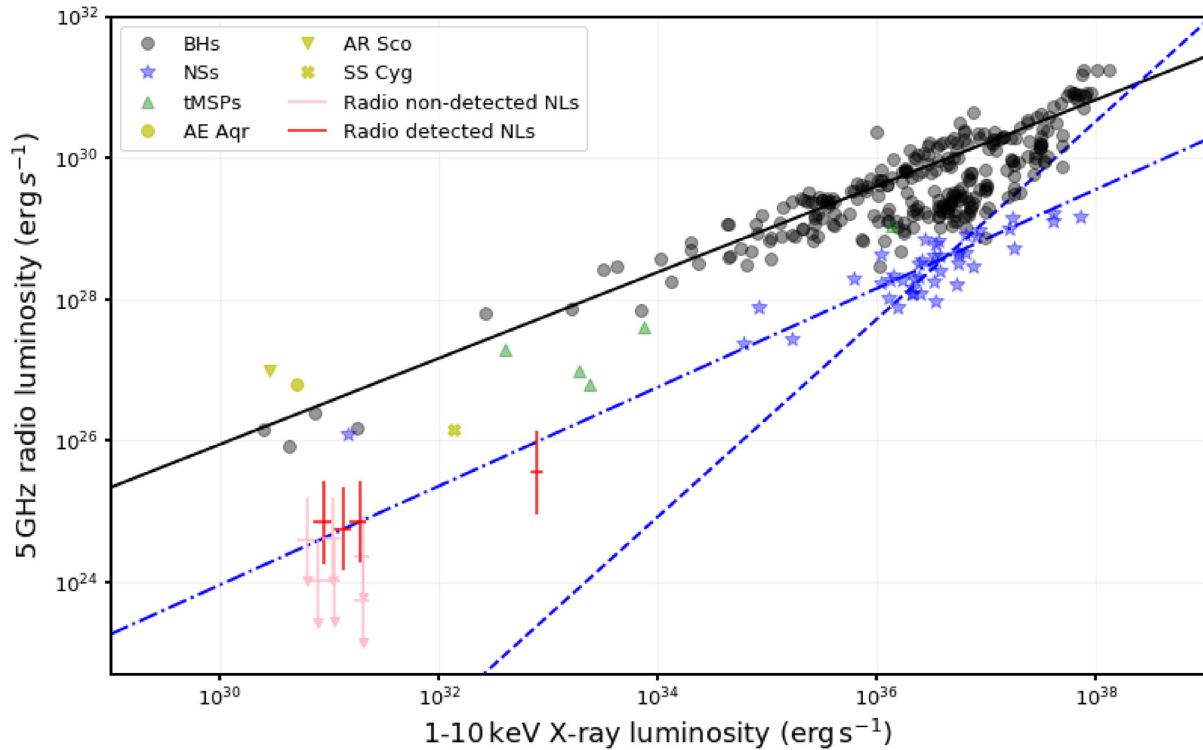
Figure 4. The logarithm of specific radio luminosities plotted versus the logarithm of specific X-ray luminosities for a number of black holes (as the black circles), neutron stars (as the blue stars), transitional millisecond pulsars (as the green triangles), our sample of detected NLs (in red) and non-detected NLs (in pink) and a few other CVs (in yellow). The X-ray:radio correlation for BHs ($L_X \propto L_R^{\sim 0.6}$; Gallo et al. 2003, 2006; Gallo et al. 2012, 2018) is plotted as a black line, and the original correlations for non-pulsating ($L_X \propto L_R^{\sim 0.7}$) and hard-state NSs ($L_X \propto L_R^{\sim 1.4}$; Migliari & Fender 2006) are also plotted as blue dot–dashed and dashed lines, respectively. Aside from our sample, these data were obtained from a data base by Bahramian et al. (2018). Sources include Gallo et al. (2003, 2006), Corbel, Koerding & Kaaret (2008), Coriat et al. (2011), Migliari, Miller-Jones & Russell (2011), Corbel et al. (2013), Gallo et al. (2014), Russell et al. (2016), Tetarenko et al. (2016a,b), Gusinskaia et al. (2017), Plotkin et al. (2017), Tudor et al. (2017), and Dinçer et al. (2018).

on, amongst other things, the presence of TiO bands in the spectrum of the secondary star, the spectral type of the secondary is estimated to be M2-5 (Hoard et al. 2001). CM Phe has a poorly sampled long-term optical light curve, and is likely a DN (see also Section 4.3). The literature contains no previous reports of radio observations of CM Phe.

3 OBSERVATIONS AND METHODS

The targets were observed using the MeerKAT radio interferometer as part of the MeerKAT large survey project for image domain explosive transients called ThunderKAT (The Hunt for Dynamic and Explosive Radio Transients using MeerKAT; Fender et al. 2017). The observations have a bandwidth of 856 MHz, centred at 1284 MHz and split into 4096 channels. Visibilities were recorded every 8 s and on average between 60 and 62 of the 64 MeerKAT antennas were available for observations. Typically, the primary calibrator was observed at the start of the observations and then for the rest of the total track length of approximately 2 h, the secondary calibrator and target were observed alternately (approximately 2 min on the secondary calibrator and 15 min on target). The details of these observations are summarized in Table 2.

The data were flagged using AOFLAGGER version 2.9.0 (Offringa 2010) and averaged by a factor 8 in frequency resulting in 512 channels, each with a bandwidth of 1.67 MHz. Data reduction and first-generation calibration were done using using standard procedures in CASA version 5.1.1. Imaging was performed using

the multifacet-based radio imaging package DDFACET (Tasse et al. 2018). Briggs weighting with a robust parameter of −0.5 and a cell size of 1.5 arcsec were chosen. Self-calibration is implemented making use of the KILLMS software and using the COHJONES solver (Smirnov & Tasse 2015). Noise was measured in the vicinity of the optical coordinates for the source, typically within the area shown in Fig. 1. All upper limits are defined as three times the rms noise level.

4 RESULTS AND DISCUSSION

This is the largest survey of NL CVs in the radio band conducted to date. We now describe our results and search for correlations between radio emission and binary system parameters, as well as emission in other wave bands.

4.1 ThunderKAT NL survey results

The results of all the MeerKAT radio observations are presented in Table 3. In total, 4 of the 11 NLs were detected: V3885 Sgr, IM Eri, RW Sex, and V603 Aql. IM Eri is detected for the first time in the radio waveband. In Fig. 1, colour maps with contours overlaid are presented for the four detected systems. Analysis of the first year of ThunderKAT data revealed an epoch-to-epoch drift in the flux scale of up to ±10 per cent, which has since been tracked down to the reference calibration method that was used. Hence, we are aware that our estimates may include a few per cent of calibration error,

though this is not the dominant source of error. The specific radio luminosities ($L_\nu = 4\pi d^2 F_\nu$, where F_ν is measured flux density) of these detected NLs range from $4.3 \pm 1.1 \times 10^{15}$ to $27 \pm 4 \times 10^{15}$ erg s^{-1} Hz^{-1}.

For the observation of V347 Pup, a weak signal with an integrated flux density of $28 \pm 14 \, \mu$Jy was present, but this does not satisfy our 5σ detection threshold. Furthermore, the offset from the optical position was ∼2 arcsec, and the signal shape is not consistent with the shape of the beam. Additionally, similar signals are also found surrounding the expected position of V347 Pup. Radio emission just above 3σ, but considerably smaller than the beam size, were detected ∼2 and ∼6 arcsec from the optical coordinates of IX Vel and LSIV 08 3, respectively. We do not consider these detections, but we report the radio flux here, in case a detection at a similar flux and with reduced noise levels is made in future.

The remaining systems were also not detected, typically with 3σ upper limits of ∼33 μJy beam^{-1}. The upper limits on the specific luminosities of the non-detected NLs range between 0.4×10^{15} erg s^{-1} Hz^{-1} (for IX Vel) and 4.6×10^{15} erg s^{-1} Hz^{-1} (for CM Phe). Radio maps for all the NLs that were not detected in our sample can be seen in Appendix A.

Coppejans et al. (2015) detected 75 per cent (3 of 4) of their sample of novalikes in the radio regime, two of which were two of the targets detected in this MeerKAT survey (V603 Aql and RW Sex). The detection rate for this MeerKAT survey is considerably lower (≈36 per cent). They did, however, select the four brightest and nearest novalikes (and the most optically luminous) from the Ritter and Kolb catalogue (Ritter & Kolb 2003) as their targets.

4.2 Spectral indices

The spectral indices ranged from -1.5 ± 1.0 to 1.2 ± 1.6 (see Table 3). These indices were calculated by first splitting the 865 MHz bandwidth into two frequency subbands, one centred at 1070 MHz and the other at 1498 MHz, and then imaging these frequency subbands to obtain a flux measurement in each. Errors are calculated using the same method as Espinasse & Fender (2018). V3885 Sgr, RW Sex, and V603 Aql have previously been detected in the radio regime. V3885 Sgr showed a spectral index of $\alpha = -0.75 \pm 0.35$ when observed by Körding et al. (2011) at 5.5 and 9 GHz, compared to our in-band value of $\alpha = -0.6 \pm 0.7$ at 1.3 GHz. Coppejans et al. (2015), observing at 4.9 GHz, found $\alpha = -0.5 \pm 0.7$ for RW Sex, and for V603 Aql $\alpha = 0.54 \pm 0.05$ during one epoch and $\alpha = 0.16 \pm 0.08$ in another. We measure $\alpha = -1.5 \pm 1.0$ for RW Sex, $\alpha = 0.2 \pm 1.1$ for V603 Aql, and $\alpha = 1.2 \pm 1.6$ for IM Eri from our in-band measurement at 1.3 GHz. The spectral indices measured from our observations are thus consistent, within the large errors, with values previously reported for the same objects using higher frequency data.

4.3 Radio emission correlations

In Fig. 2, we plot radio luminosity as a function of absolute magnitude [Ritter & Kolb 2003, or Variable Star Index (VSX)] for our sample of 11 NLs, as well as for all the previous detections of non-magnetic CVs (DNe in grey and NLs in black). The radio luminosities of our sample are not at the same frequency as that of previous detections. There is still no statistically significant correlation between the radio and optical luminosities for the existing sample. This plot does, however, show that all the NLs that were detected by MeerKAT (as well as previous radio detections of non-magnetic CVs made by other authors) displayed a relatively

high specific optical luminosity $\gtrsim 2.2 \times 10^{18}$ erg s^{-1} Hz^{-1} (corresponding to $M_V \lesssim 6.0$). Yet, not all the optically luminous NLs were detected at radio wavelengths – notably IX Vel, LSIV -08 3, and V341 Ara. These three systems do not seem to share any common attributes (such as winds or spiral shocks) that would set them apart from the detected NLs.

V5662 Sgr and CM Phe have optical luminosities significantly below those of the rest of the sample, and although they are currently classified as NLs, they are likely DNe in which outbursts have thus far been missed (see also Thorstensen 2020). Both have poorly sampled long-term light curves, and absolute magnitudes that are consistent with those of quiescent DN at their respective periods (e.g. Warner 1987).

In Fig. 3 radio luminosity is plotted as a function of orbital period for our sample of 11 NLs, as well as for all the previous detected non-magnetic CVs. The MeerKAT survey has evidently been effective at sampling the entire orbital period parameter space. Throughout the range of orbital periods, radio luminosities and upper limits remain comparable.

Radio luminosities have been plotted as a function of X-ray luminosities for a number of black holes (BHs), neutron stars (NSs), transitional millisecond pulsars, a few CVs,[3] and our sample of 11 NLs in Fig. 4. These data are obtained from a data base compiled by Bahramian et al. (2018; see Fig. 4 for references). The famous X-ray:radio correlation for BHs ($L_X \propto L_R^{\sim 0.6}$; Gallo, Fender & Pooley 2003; Gallo et al. 2006; Gallo, Miller & Fender 2012; Gallo, Degenaar & van den Eijnden 2018) is plotted as a black line, and the correlations for non-pulsating ($L_X \propto L_R^{\sim 0.7}$) and hard-state NSs ($L_X \propto L_R^{\sim 1.4}$; Migliari & Fender 2006) are also plotted as the blue dot–dashed and dashed lines, respectively. The detected NLs from our survey are plotted in red, and the non-detected NLs in pink. The uncertainties on the x-axis correspond to *ROSAT* X-ray luminosities (Voges et al. 1999) assuming thermal bremsstrahlung with kT ranging from $5 - 20$ keV (Pretorius & Knigge 2011), while the uncertainties on the y-axis correspond to the MeerKAT radio luminosities of the NLs scaled from 1.3 to 5 GHz, using spectral indices in the range $-1 < \alpha < 1$. We note that, unlike the other points on this plot, the radio and X-ray observations are of course not even quasi-simultaneous; however, none of the these NLs are known to display changes in their accretion state. The four NLs that have been detected are surprisingly well described (qualitatively at least) by the non-pulsating NS correlation. The remainder of the sample does, however, fall below this correlation line, possibly by as much as an order of magnitude in radio luminosity, or even more, but might well still follow other NS X-ray:radio relations that have been proposed.

While the correlation between the X-ray and radio emission is certainly significant for BHs (see e.g. Tremou et al. 2020 for a recent discussion), the picture is more complicated in the case of NS systems. The correlation has been studied in depth in only a few individual systems (Migliari et al. 2003; Tudose et al. 2009; Tetarenko et al. 2016a; Gusinskaia et al. 2020), with different values of the power-law index proposed by different groups and in different sources. More recently a 'universal' NS correlation index of 0.44 has been suggested (Gallo et al. 2018, although see Tudor et al. 2017).

---

[3]These systems all belong to other classes of accreting WDs than NLs. SS Cyg is a DN, AE Aqr is a probable magnetic propeller (Wynn, King & Horne 1997), and AR Sco is interpreted to be a WD pulsar (Marsh et al. 2016).
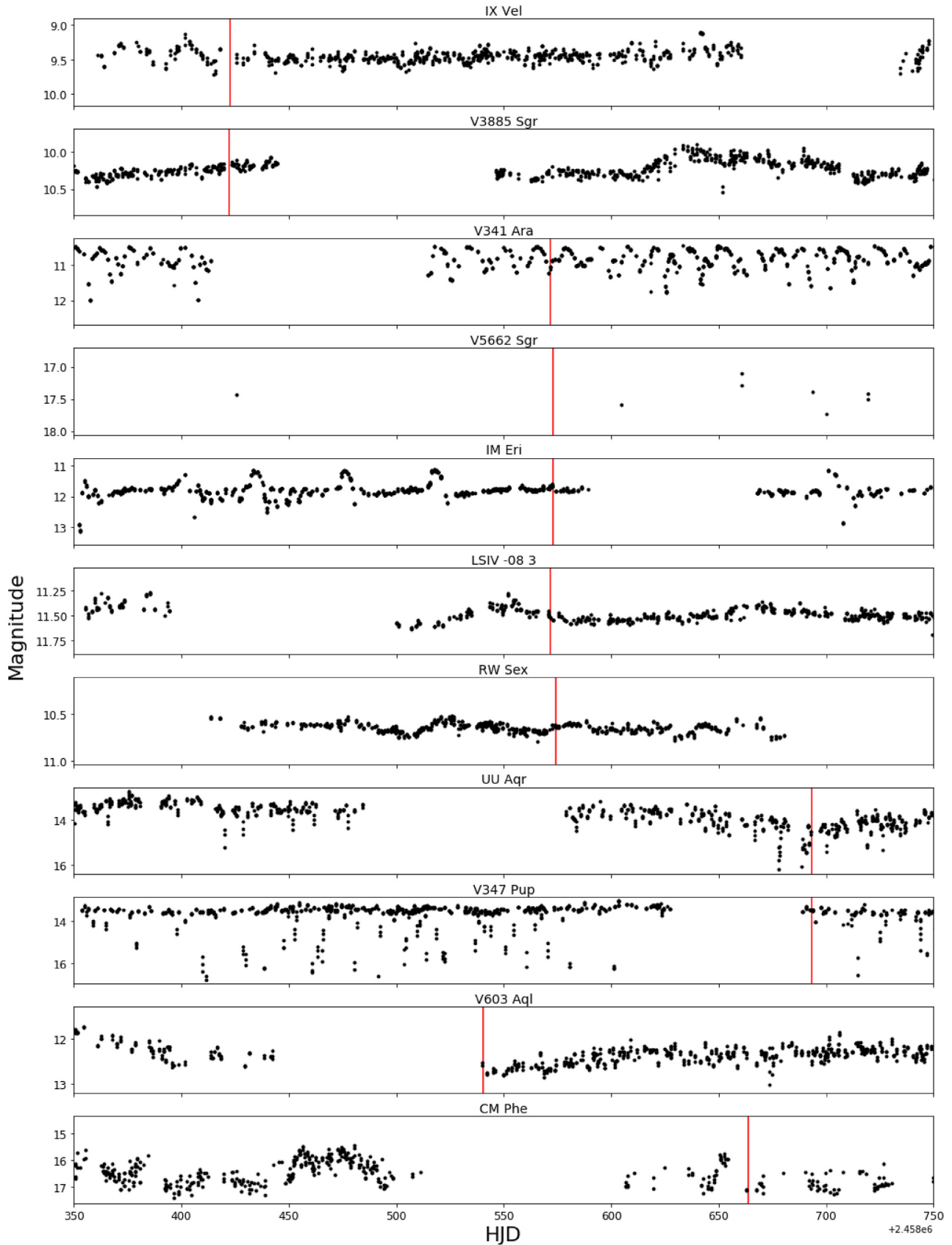
Figure 5. Optical light curves of our sample, covering 400 d, from the ASAS-SN variable star data base (Shappee et al. 2014; Kochanek et al. 2017). The vertical red lines indicate the epochs of radio observation reported here. With the exception of V5662 Sgr, the optical light curves are well enough sampled to show that none of our targets were in a low state during our radio observations. Note the IW And-type photometric behaviour discussed by Kato et al. (2020) in the light curve of IM Eri.
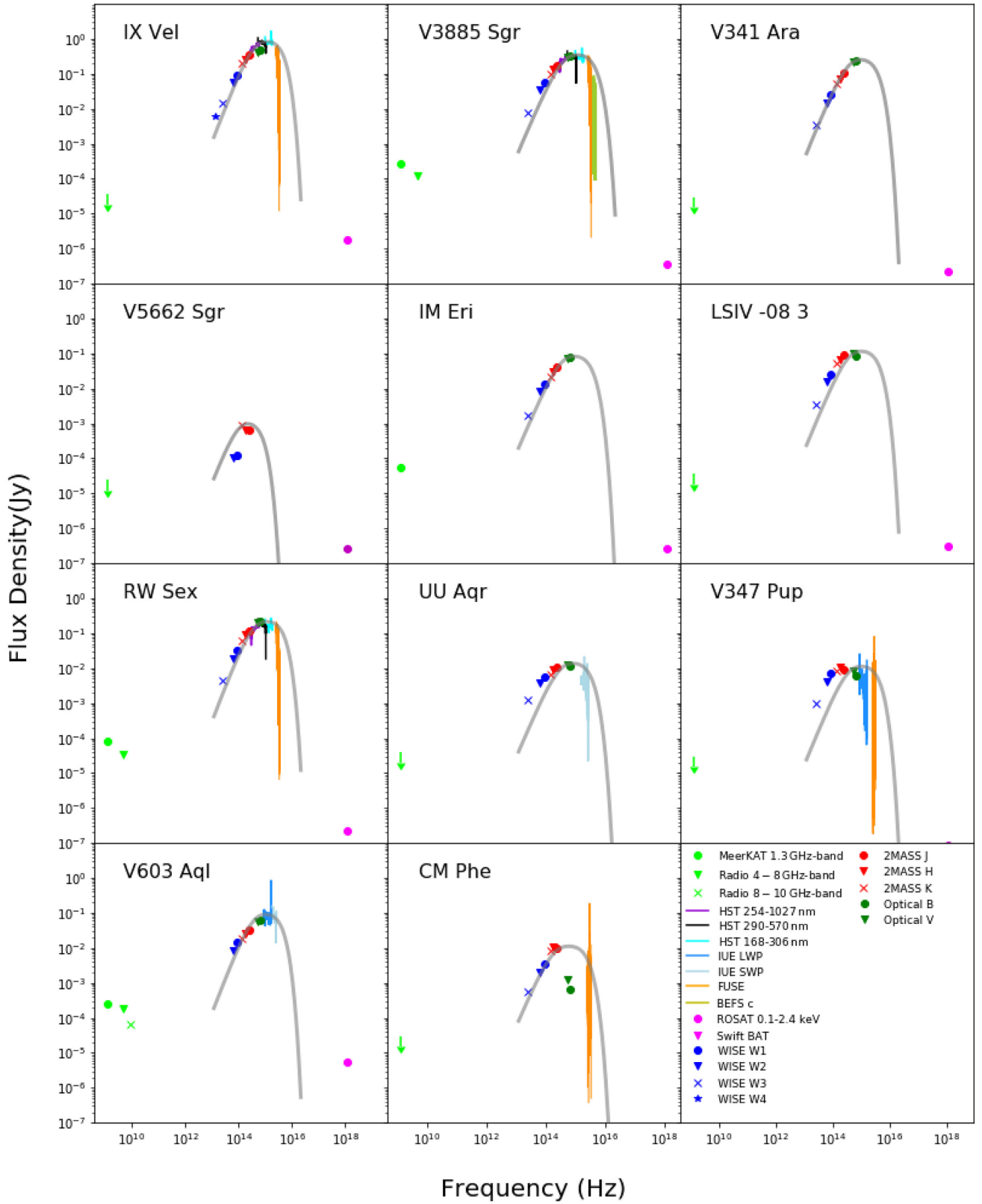
Figure 6. SEDs for our NL sample, constructed using our radio observations as well as published data from a large collection of earlier observations. A blackbody disc model with appropriate system parameters where possible, and the mass accretion rate which gives rise to a curve that best resembles the data, is overplotted. Refer to Table 4 for the system parameters and the text for more detail.

Table 4. The system parameters used for the blackbody disc models shown in Fig. 6. References for the values that are available in the literature may be found in Section 2.

Name	M_1 (M$_\odot$)	M_2 (M$_\odot$)	i (°)	$\dot{M}$ ($\times 10^{-9}$ M$_\odot$ yr^{-1})
IX Vel	0.8	0.52	57	7
V3885 Sgr	0.675	0.473	60	8
V341 Ara	0.75[a]	0.27[a]	30	3.5
V5662 Sgr	0.75[a]	0.09[a]	57[a]	0.005
IM Eri	0.75[a]	0.24[a]	57[a]	2.5
LS IV -08 3	0.75[a]	0.45[a]	57[a]	5
RW Sex	0.84	0.62	34	8
UU Aqr	0.67	0.2	78	2
V347 Pup	0.63	0.52	84	6
V603 Aql	1.2	0.29	13	3
CM Phe	0.75[a]	0.5[b]	57[a]	0.7

[a]Value not known and estimated from Knigge (2006), Knigge, Baraffe & Patterson (2011), or Warner (1995). See text for more detail.
[b]See the discussion in Section 4.5.

In BH XRBs, the X-ray emission generally serves as a reliable proxy for the accretion rate, with non-thermal emission from the inner accretion flow dominating during low/hard states (Yuan & Narayan 2014). It is during these low states that synchrotron emitting jets are observed at radio wavelengths (e.g. Corbel et al. 2000; Fender 2001). For CVs, the accretion light peaks in the UV, rather than X-ray, band. Our data of course also do not allow us to demonstrate that jets are responsible for the radio emission in NLs. Given this, together with the ongoing debate surrounding the X-ray:radio correlation for NS systems, and the fact that our radio and X-ray observations are not contemporaneous, we caution against overinterpreting the position of our NLs in Fig. 4. Nevertheless, Fig. 4 serves to show, at the very least, that NLs can introduce confusion when classifying very low-luminosity NS XRBs using their X-ray:radio properties.

In Fig. 5, the long-term ASAS-SN optical light curves of these 11 NLs are shown (Shappee et al. 2014; Kochanek et al. 2017). None of the NLs in the sample are known to be a VY Scl star that would exhibit significant low states (anti-DN outbursts) and from these light curves it is evident that none of the NLs were observed during a time of anomalous optical activity. There is thus no easy explanation as to why the three previously mentioned optically bright systems (IX Vel, LSIV -08 3, and V341 Ara) are radio faint, while the other optically bright systems are detected.

4.4 Broad-band SEDs

The broad-band spectral energy distributions (SEDs) of the NL sample are shown in Fig. 6. As expected, each broad SED shows, in the UV to IR wavebands, a component that appears to be dominated by blackbody emission from an accretion disc. Lower and higher energy emission, belonging to other components, can also be seen. Warner (2006) gives an overview of the emission observed in CVs across the whole electromagnetic spectrum. All three systems with multiple detections at different radio wavelengths exhibit a radio flux that is decreasing with increasing frequency, i.e. a negative spectral index α. In Section 4.2 above, we reported both negative and positive in-band spectral indices. The broader frequency coverage of the combined MeerKAT and VLA/ATCA data should be a more reliable indication of α, but this discrepancy may also be caused by variability on both long and short time-scales. Coppejans et al. (2015) observed that the spectral index of V603 Aql differed in two

different epochs of observation, a week apart, and that the spectral index of TT Ari changed during a flare.

4.5 Mass accretion rates

We have overplotted a blackbody model of an accretion disc, using input system parameters summarized in Table 4, many of which are taken from the literature and mentioned in the relevant subsections of Section 2. The curves shown in Fig. 6 are not fits to the SEDs, and do not include any contribution from the WD or donor star. We simply varied the input $\dot{M}$ of the disc model, and selected the value that produces the blackbody disc spectrum that most resembles the observed SED. Those accretion rates are given in Table 4 for each system. The blackbody model calculates the shape of a blackbody for a range of temperatures dependent on the viscous dissipation rate D of an optically thick Keplerian accretion disc:

$$D(R) = \frac{3GM\dot{M}}{4\pi R^3}\left[1 - \left(\frac{R_*}{R}\right)^{1/2}\right], \tag{1}$$

where G is the gravitational constant, R is the radius of the disc, M is the WD mass, $\dot{M}$ is the accretion rate, and R_* is the WD radius.

In the case where system parameters were not known (and thus not mentioned in Section 2), we selected an inclination of $i = 57°$ (Warner 1995), $M_1 = 0.75$ M$_\odot$ (Knigge 2006), and estimated M_2 using the binary and evolution parameters along the revised model track (Knigge et al. 2011). CM Phe has an orbital period above 6 h, implying that it likely has a secondary star that has evolved off the main sequence. The calculated blackbody is not very sensitive to M_2, and we will therefore simply assume $M_2 = 0.5$ M$_\odot$ for CM Phe (corresponding roughly to an M0 dwarf); see Hoard et al. (2001) for a more complete discussion.

The inner radius of the disc is set to be 7000 km (the approximate radius for an average WD), and the outer radius is defined as $0.7R_{L1}$ where R_{L1} is the Roche lobe radius of the primary (Harrop-Allin & Warner 1996). The Roche lobe radius of the primary was calculated using equation (2; Silber 1992):

$$\frac{R_{L1}}{a} = \left(1.0015 + q^{0.4056}\right)^{-1}, \tag{2}$$

where a is the period-dependent orbital separation and $q = M_2/M_1$. This equation is valid for $0.04 \leq q \leq 1$ with an error <1 per cent.

For V347 Pup and UU Aqr, the blackbody model clearly does not resemble the observed SED. Both of these systems have high inclinations ($i > 75°$), and it is thus possible that the disc is occulted to some degree, or the disc rim is being observed, which is not consistent with a blackbody. Mauche et al. (1994) noted that V347 Pup has an exceptionally red continuum spectrum for a high-$\dot{M}$ CV – interpreted as the result of a self-occulted accretion disc.

Fig. 7 shows the blackbody component of the detected subsample with the most suitable accretion rate as a solid grey line, and accretion rates 25 per cent greater and smaller, respectively, as the dashed grey lines overplotted on the SEDs.

We find that for IX Vel $\dot{M} \approx 7 \times 10^{-9}$ M$_\odot$ yr^{-1} shows good agreement with the observed SED. This is closer to the value of $(7.9 \pm 1.0) \times 10^{-9}$ M$_\odot$ yr^{-1}, which was proposed by Beuermann & Thomas (1990), than to 5×10^{-9} M$_\odot$ yr^{-1}, which was proposed by Linnell et al. (2007), however, they noted that their model only excludes estimates above 8×10^{-9} M$_\odot$ yr^{-1}, in which case our value is still consistent.

For V3885 Sgr, $(5 \pm 2) \times 10^{-9}$ M$_\odot$ yr^{-1} is proposed by Linnell et al. (2009). The SED agrees better with a slightly higher value of
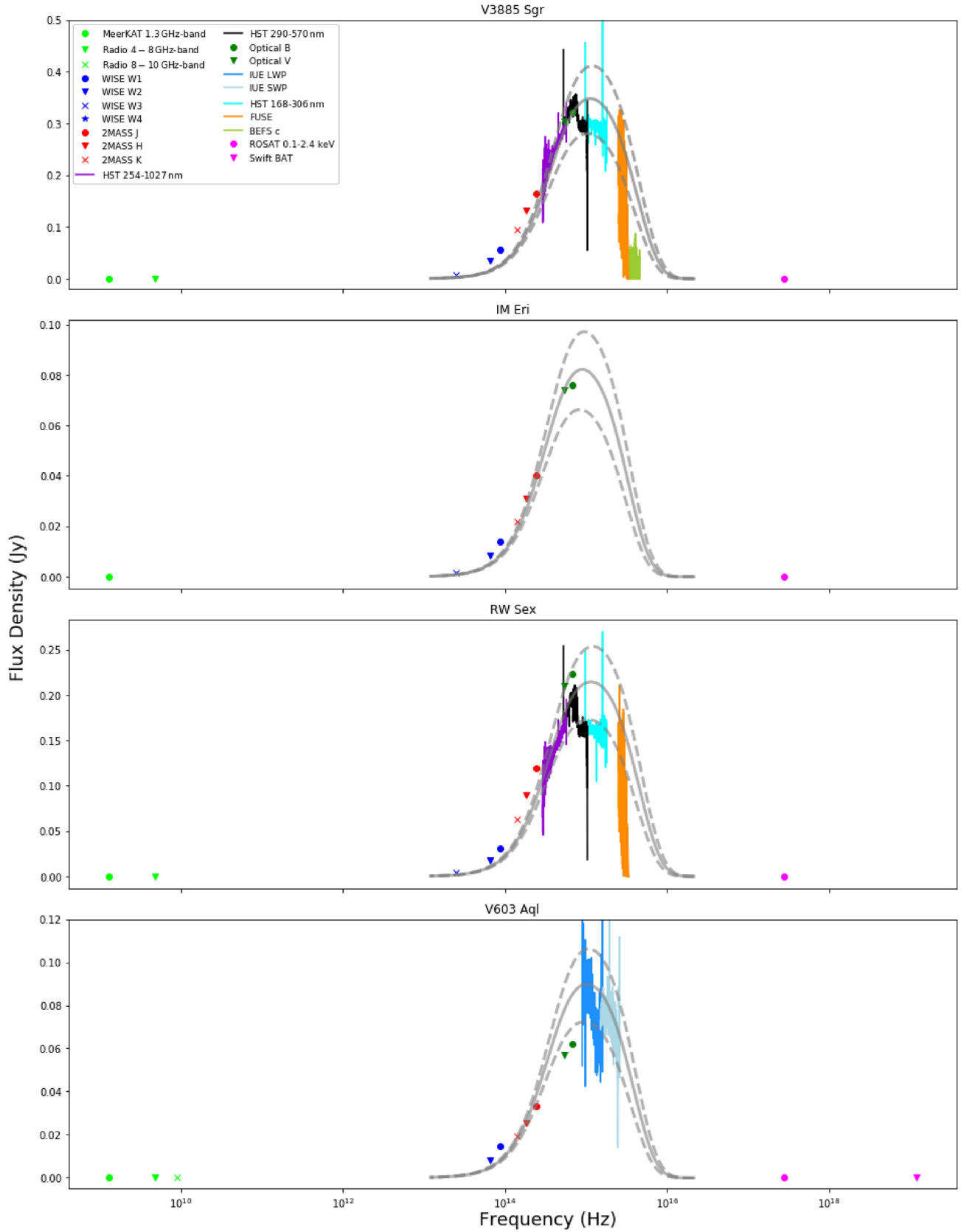
Figure 7. SEDs for the detected NLs in our sample. A blackbody disc model is overplotted, with the optimal accretion rate to resemble the data as a solid grey line, and accretion rates 25 per cent greater and smaller as the dashed grey lines. Note that the $\dot{M}$ we derive for IM Eri is particularly uncertain, since there are no UV data available (see Fig 6), and since the binary parameters relevant to the blackbody model include an assumed typical inclination and WD mass. None the less, IM Eri is the least optically luminous system we detected in the radio.
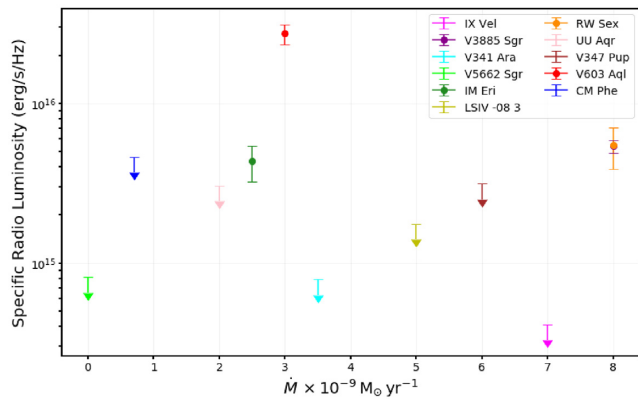
Figure 8. The logarithm of specific radio luminosities plotted versus $\dot{M}$ suggested by the observed SEDs and the blackbody disc model for our sample of NLs. As illustrated in Fig. 7, the uncertainty in $\dot{M}$ is roughly 25 per cent. The symbols for RW Sex and V3885 Sgr overlap, so only error bars for the latter can be seen.

$8 \times 10^{-9}\,\mathrm{M_\odot\,yr^{-1}}$, but Fig. 7 shows that a value of $6 \times 10^{-9}\,\mathrm{M_\odot\,yr^{-1}}$ is still reasonable.

According to models by Linnell et al. (2010), the optimal $\dot{M}$ for RW Sex is $5.75 \times 10^{-9}\,\mathrm{M_\odot\,yr^{-1}}$. They used a *Hipparcos* parallax to obtain a distance of 289 pc (now known to be $\approx$22 per cent too large). Other estimates are as high as $1 \times 10^{-8}\,\mathrm{M_\odot\,yr^{-1}}$ (Greenstein & Oke 1982). We find that $\dot{M} \approx 8 \times 10^{-9}\,\mathrm{M_\odot\,yr^{-1}}$ best suits the SED.

For UU Aqr $\dot{M} = 1.0^{+0.6}_{-0.4} \times 10^{-9}\,\mathrm{M_\odot\,yr^{-1}}$ has been proposed (Baptista et al. 1996). From our model we find $\dot{M} \approx 2 \times 10^{-9}\,\mathrm{M_\odot\,yr^{-1}}$.

V603 Aql has been estimated to have $\dot{M}$ ranging from $9.2 \times 10^{-9}\,\mathrm{M_\odot\,yr^{-1}}$ to $9.47 \times 10^{-8}\,\mathrm{M_\odot\,yr^{-1}}$ (Retter & Naylor 2000). Our blackbody disc that best resembles the SED of V603 Aql has an $\dot{M} \approx 3 \times 10^{-9}\,\mathrm{M_\odot\,yr^{-1}}$ – significantly lower than Retter & Naylor, but still of the same order of magnitude.

In general, the accretion rates suggested by the observed SEDs and our blackbody disc model are slightly higher than what has previously been suggested by other authors, and our blackbody disc model tends to marginally underestimate the higher energy side of the disc component. We note that we have not incorporated any UV extinction into our blackbody disc models. Furthermore, we have no contributions to the UV to IR emission from the stellar components, but instead assume that those are small compared to the disc emission in NL systems.

In Fig. 8, we plot specific radio luminosity as a function of our rough $\dot{M}$ estimates. Although there is no clear correlation between these two quantities, we expect this to mirror what is illustrated in Fig. 2. In other words, since, for our sample, high optical luminosity is a necessary condition for a radio detection, it should also be the case that below some $\dot{M}$, our sources are not detected in the radio. This is seen in Fig. 8.

5 CONCLUSIONS

We have presented the results of the largest radio survey of nova-like CVs to date. We observed 11 systems, all within 350 pc, with the MeerKAT radio interferometer, and detected radio emission from four of them. Our main results are summarized next:

(i) The four NL systems that have been detected in this survey are IM Eri, RW Sex, V3885 Sgr, and V603 Aql.

(ii) The specific radio luminosities of the NLs detected in our sample are between $4.3 \pm 1.2 \times 10^{15}$ and $27 \pm 4 \times 10^{15}\,\mathrm{erg\,s^{-1}\,Hz^{-1}}$.

(iii) Upper limits on the specific radio luminosities of NLs not detected in our sample are between $0.4 \times 10^{15}\,\mathrm{erg\,s^{-1}\,Hz^{-1}}$ for IX Vel and $4.6 \times 10^{15}\,\mathrm{erg\,s^{-1}\,Hz^{-1}}$ for CM Phe. These non-detections are not explained by a deep low optical state.

(iv) The spectral indices of the radio emission from our detected NLs ranged from -1.5 ± 1.0 to 1.2 ± 1.6, but a trend $\alpha < 0$ is observed when including data from the VLA or ATCA.

(v) Radio emission is only observed in systems with a high specific optical luminosity $\gtrsim 2.2 \times 10^{18}\,\mathrm{erg\,s^{-1}\,Hz^{-1}}$ at our radio detection limits (corresponding to $M_V \lesssim 6.0$).

(vi) The X-ray and radio emission of our detected NLs lie on the same power law that has previously been proposed for non-pulsating NS low-mass XRBs ($L_X \propto L_R^{\sim 0.7}$).

(vii) We have plotted SEDs of the 11 NLs, overlayed with a simple $\dot{M}$-dependent blackbody disc model. We find that for most of the systems $\dot{M} \sim 10^{-9}\,\mathrm{M_\odot\,yr^{-1}}$ is consistent with the apparently blackbody spectral component.

(viii) Prior to this work eight NLs have been observed, seven in the last decade, of which four have been detected. We have observed seven additional NL systems for the first time, and contributed one novel detection (IM Eri).

Some of the research in this paper is based on observations made with the NASA/ESA *Hubble Space Telescope*, and obtained from the Hubble Legacy Archive, which is a collaboration between the Space Telescope Science Institute (STScI/NASA), the Space Telescope European Coordinating Facility (ST-ECF/ESAC/ESA), and the Canadian Astronomy Data Centre (CADC/NRC/CSA).

This publication has used data products from the Two Micron All Sky Survey, which is a joint project of the University of Massachusetts and the Infrared Processing and Analysis Center/California Institute of Technology, funded by NASA and the National Science Foundation.

This publication has used data products from the Wide-field Infrared Survey Explorer, which is a joint project of the University of California, Los Angeles, and the Jet Propulsion Laboratory/California Institute of Technology, funded by NASA.

Some of the data used were obtained from the Mikulski Archive for Space Telescopes. STScI is operated by the Association of Universities for Research in Astronomy, Inc., under NASA contract NAS5-26555.

This research has used ASTROPY,[4] a community-developed core PYTHOn package for Astronomy (Robitaille et al. 2013; Price-Whelan et al. 2018). This research has used APLPY, an open-source plotting package for PYTHON (Robitaille & Bressert 2012).

DATA AVAILABILITY

The MeerKAT data presented in this article are subject to the standard data access policy of the South African Radio Astronomy Observatory.

REFERENCES

Ak T., Bilir S., Ak S., Eker Z., 2008, New Astron., 13, 133
Arenas J., Catalan M. S., Augusteijn T., Retter A., 2000, MNRAS, 311, 135
Armstrong E. et al., 2013, MNRAS, 435, 707
Bahramian A. et al., 2018, Radio/X-ray correlation database forX-ray binaries,, http://dx.doi.org/10.5281/zenodo.1252036
Baptista R., Bortoletto A., 2008, ApJ, 676, 1240
Baptista R., Steiner J. E., Cieslinski D., 1994, ApJ, 433, 332
Baptista R., Steiner J. E., Horne K., 1996, MNRAS, 282, 99
Barrett P. E., Dieck C., Beasley A. J., Singh K. P., Mason P. A., 2017, AJ, 154, 252
Benz A. O., Fürst E., Kiplinger A. L., 1983, Nature, 302, 45
Beuermann K., Thomas H.-C., 1990, A&A, 230, 326
Beuermann K., Stasiewski U., Schwope A. D., 1992, A&A, 256, 433
Bond H. E., Miszalski B., 2018, PASP, 130, 094201
Buckley D. A. H., Sullivan D. J., Remillard R. A., Tuohy I. R., Clark M., 1990, ApJ, 355, 617
Coppejans D., Knigge C., 2020, arXiv e-prints, arXiv:2003.05953
Coppejans D. L., Körding E. G., Miller-Jones J. C. A., Rupen M. P., Knigge C., Sivakoff G. R., Groot P. J., 2015, MNRAS, 451, 3801
Coppejans D. L. et al., 2016, MNRAS, 463, 2229
Corbel S., Fender R. P., Tzioumis A. K., Nowak M., McIntyre V., Durouchoux P., Sood R., 2000, A&A, 359, 251
Corbel S., Koerding E., Kaaret P., 2008, MNRAS, 389, 1697
Corbel S., Coriat M., Brocksopp C., Tzioumis A. K., Fender R. P., Tomsick J. A., Buxton M. M., Bailyn C. D., 2013, MNRAS, 428, 2500
Cordova F. A., Hjellming R. M., Mason K. O., 1983, PASP, 95, 69
Coriat M. et al., 2011, MNRAS, 414, 677
Coriat M., Fender R. P., Dubus G., 2012, MNRAS, 424, 1991
Dinçer T., Bailyn C. D., Miller-Jones J. C. A., Buxton M., MacDonald R. K. D., 2018, ApJ, 852, 4

Espinasse M., Fender R., 2018, MNRAS, 473, 4122
Fender R. P., 2001, MNRAS, 322, 31
Fender R., et al., 2017, arXiv e-prints, arXiv:1711.04132
Fender R., Bright J., Mooley K., Miller-Jones J., 2019, MNRAS, 490, L76
Frew D. J., 2008, PhD thesis, Department of Physics, Macquarie University
Fuerst E., Benz A., Hirth W., Kiplinger A., Geffert M., 1986, A&A, 154, 377
Gaia Collaboration, 2016, A&A, 595, A1
Gaia collaboration, 2018, A&A, 616, A1
Gallo E., Fender R., Pooley G., 2003, MNRAS, 344, 60
Gallo E., Fender R., Miller-Jones J., Merloni A., Jonker P., Heinz S., Maccarone T., van der Klis M., 2006, MNRAS, 370, 1351
Gallo E., Miller B. P., Fender R., 2012, MNRAS, 423, 590
Gallo E. et al., 2014, MNRAS, 445, 290
Gallo E., Degenaar N., van den Eijnden J., 2018, MNRAS, 478, L132
Greenstein J. L., Oke J. B., 1982, ApJ, 258, 209
Gusinskaia N. V. et al., 2017, MNRAS, 470, 1871
Gusinskaia N. V. et al., 2020, MNRAS, 492, 2858
Harrop-Allin M. K., Warner B., 1996, MNRAS, 279, 219
Hartley L. E., Murray J. R., Drew J. E., Long K. S., 2005, MNRAS, 363, 285
Hillwig T., Livio M., Honeycutt R., 2004, PASP, 116, 397
Hoard D., Wachter S., Kim-Quijano J., 2001, PASP, 113, 482
Honeycutt R. K., Robertson J. W., Turner G. W., 1998, AJ, 115, 2527
Jaidee S., Lyngå G., 1969, Ark. Astron., 5, 345
Johnson C. B., Schaefer B. E., Kroll P., Henden A. A., 2014, ApJ, 780, L25
Jonas J. L., 2009, Proc. IEEE, 97, 1522
Kato T. et al., 2020, PASJ, 72, 11
Knigge C., 2006, MNRAS, 373, 484
Knigge C., Baraffe I., Patterson J., 2011, ApJS, 194, 28
Kochanek C. S. et al., 2017, PASP, 129, 104502
Körding E., Rupen M., Knigge C., Fender R., Dhawan V., Templeton M., Muxlow T., 2008, Science, 320, 1318
Körding E. G., Knigge C., Tzioumis T., Fender R., 2011, MNRAS, 418, L129
Linnell A. P., Godon P., Hubeny I., Sion E. M., Szkody P., 2007, ApJ, 662, 1204
Linnell A. P., Godon P., Hubeny I., Sion E. M., Szkody P., Barrett P. E., 2009, ApJ, 703, 1839
Linnell A. P., Godon P., Hubeny I., Sion E. M., Szkody P., 2010, ApJ, 719, 271
Luri X. et al., 2018, A&A, 616, A9
Marsh T. R. et al., 2016, Nature, 537, 374
Mauche C. W., Raymond J. C., Buckley D. A. H., Mouchet M., Bonnell J., Sullivan D. J., Bonnet-Bidaud J.-M., Bunk W. H., 1994, ApJ, 424, 347
Migliari S., Fender R. P., 2006, MNRAS, 366, 79
Migliari S., Fender R., Rupen M., Jonker P., Klein-Wolt M., Hjellming R., van der Klis M., 2003, MNRAS, 342, L67
Migliari S., Miller-Jones J. C., Russell D. M., 2011, MNRAS, 415, 2407
Miller-Jones J. C. A. et al., 2011, in Romero G.E., Sunyaev R.A., Belloni T.,, eds., Proc. IAU Symp. 275, Jets at All Scales. Cambridge Univ. Press, Cambridge, p. 224
Mooley K. P. et al., 2017, MNRAS, 467, L31
Nelson R. F., Spencer R. E., 1988, MNRAS, 234, 1105
Offringa A. R., 2010, Astrophysics Source Code Library, record ascl:1010.017
Osaki Y., 1974, PASJ, 26, 429
Osaki Y., 1996, PASP, 108, 39
Pala A. F., 2019, Technical report, Fundamental properties of Cataclysmic Variables from Gaia DR2.
Payne-Gaposchkin C., 1964, The Galactic Novae. Dover Press, New York
Peters C., Thorstensen J., 2006, PASP, 118, 687
Plotkin R. M. et al., 2017, ApJ, 848, 92
Pretorius M. L., Knigge C., 2011, MNRAS, 419, 1442
Price-Whelan A. M. et al., 2018, AJ, 156, 123
Prinja R. K., Rosen R., 1995, MNRAS, 273, 461
Retter A., Naylor T., 2000, MNRAS, 319, 510
Ribeiro F. M. A., Diaz M. P., 2007, AJ, 133, 2659

[4]http://www.astropy.org

Ritter H., Kolb U., 2003, A&A, 404, 301
Robitaille T., Bressert E., 2012, Astrophysics Source Code Library, record ascl:1208.017
Robitaille T. P. et al., 2013, A&A, 558, A33
Russell T. D. et al., 2016, MNRAS, 460, 3720
Shappee B. J. et al., 2014, ApJ, 788, 13
Silber A. D., 1992, PhD Thesis, Massachusetts Institute of Technology
Sion E. M., 1985, ApJ, 292, 601
Smirnov O., Tasse C., 2015, MNRAS, 449, 2668
Sokoloski J. L., Rupen M. P., Mioduszewski A. J., 2008, ApJ, 685, L137
Stark M. A., Wade R. A., Thorstensen J. R., Peters C. S., Smith H. A., Miller R. D., Green E. M., 2008, AJ, 135, 991
Still M. D., Buckley D. A. H., Garlick M. A., 1998, MNRAS, 299, 545
Tappert C., Augusteijn T., Maza J., 2004, MNRAS, 354, 321
Tasse C. et al., 2018, A&A, 611, A87
Taylor A. R., Seaquist E. R., Mattei J. A., 1986, Nature, 319, 38
Tetarenko A. J. et al., 2016a, MNRAS, 460, 345
Tetarenko B. E. et al., 2016b, ApJ, 825, 10
Thoroughgood T. D. et al., 2005, MNRAS, 357, 881
Thorstensen J. R., 2020, arXiv e-prints, arXiv:2005.02150

Tomov T., Munari U., Kolev D., Tomasella L., Rejkuba M., 1998, A&A, 333, L67
Torbett M. V., Campbell B., 1987, ApJ, 318, L29
Tremou E. et al., 2020, MNRAS, 493, L132
Tudor V. et al., 2017, MNRAS, 470, 324
Tudose V., Fender R. P., Linares M., Maitra D., van der Klis M., 2009, MNRAS, 400, 2111
Vande Putte D., Smith R. C., Hawkins N. A., Martin J. S., 2003, MNRAS, 342, 151
Voges W. et al., 1999, A&A, 349, 389
Warner B., 1987, MNRAS, 227, 23
Warner B., 1995, Cataclysmic Variable Stars. Cambridge Univ. Press, Cambridge
Warner B., 2006, J. Am. Assoc. Var. Star Obs., 35, 98
Wynn G. A., King A. R., Horne K., 1997, MNRAS, 286, 436
Yuan F., Narayan R., 2014, ARA&A, 52, 529

APPENDIX A: NON-DETECTION RADIO MAPS

Colour radio maps with overlayed contours of the seven non-detected NLs are presented in Figure A1.
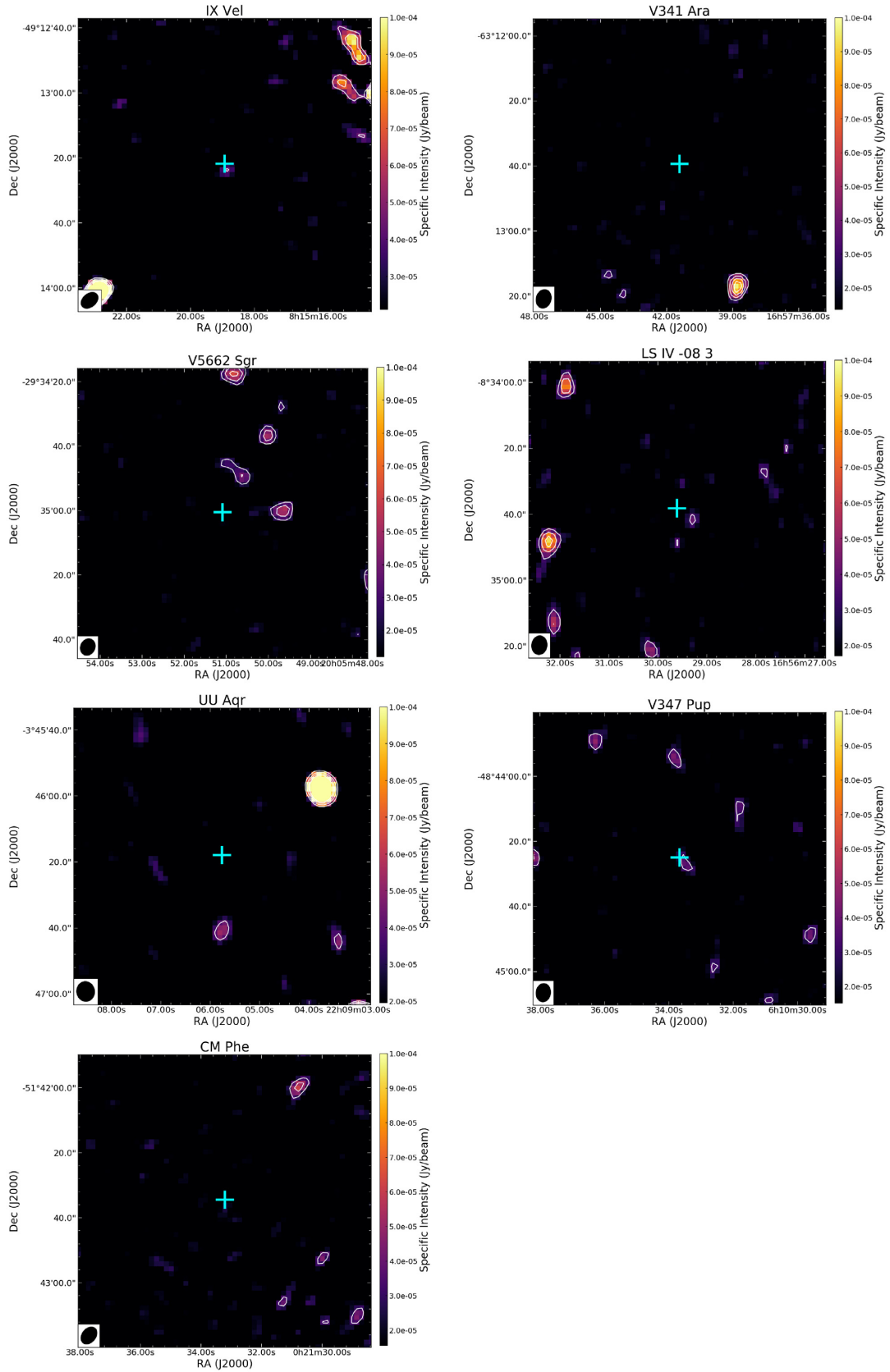
Figure A1. Radio colour maps and contours of the remaining undetected NLs. Contour levels are at 3σ, 5σ, 7σ, and 9σ levels. The cyan plus indicates the position of the optical coordinates and does not correspond to the error bars. These images are 1.5 arcmin × 1.5 arcmin in size and the shape of the synthesized beam is shown in the bottom left corner. The beam dimensions are given in Table 3. North is up and east to the left.

This paper has been typeset from a TEX/LATEX file prepared by the author.